

A theoretical investigation of chromaticity

L. Lindegren, Lund Observatory

GAIA-CA-TN-LU-LL-064-1 (15 November 2005)

ABSTRACT. Some general results are derived on the chromatic properties of diffraction images for arbitrary wavefront errors. Although the theoretical results are probably of limited practical use, they are nevertheless important for understanding the behaviour of actual centroiding algorithms in real optical systems. The main results are: (1) the centre-of-gravity (CoG) of the diffraction image can only be defined as a mathematical limit, and in practice cannot be computed to reasonable accuracy and stability in presence of noise; (2) for arbitrary wavefront errors, the limiting CoG is independent of wavelength and thus without chromaticity; (3) practically useful centroiding algorithms exhibit chromatic behaviour which depends strongly on the details of the algorithm and wavefront errors. Certain limiting behaviours are identified and explained.

1 Introduction

A fundamental step in the Gaia data analysis is the so-called image centroiding, where a given (theoretical, empirical, or *ad hoc*) image profile is fitted to the observed CCD pixel values in order to estimate the precise location of the image centre with respect to the pixel mesh.¹ That the precise centroid location depends on the spectral composition of the detected light, an effect known as *chromaticity*, has long been recognised as one of the more difficult aspects of the instrument calibration. The problem has been treated in several technical notes which describe the phenomenon, its calculation, calibration, photometric system issues, and associated requirements on the optical design [2, 3, 4, 6, 7].

The sensitivity of the derived chromaticity to the precise definition of the centroid was emphasised in several places. A ‘typical’ definition of the centroid may involve fitting a gaussian function of given width to the observed profile. (The fact that real PSFs are far from gaussian is irrelevant here: such a definition can nevertheless provide a reasonable location estimate in terms of precision. The fitting is equivalent to finding the maximum cross-correlation between the observed data and the gaussian template.) In such cases the centroid position is found to depend sensitively on the chosen width of the gaussian. Typical curves for the centroids of monochromatic images are found in Fig. 2 of [4]. In the figure it is seen that the variation with wavelength is much less when using a wide gaussian (e.g., standard width $s = 2$ pixels) than with a narrow gaussian (e.g., $s = 0.5$). In practice the width must be adjusted to minimise the sensitivity of the centroid to photon and read-out noise, which requires a width slightly larger than that of the actual PSF ($s = 1$ to 1.5).

¹We neglect here a number of practical issues related to the actual detection of the image (sampling, TDI operation of the CCD, pixel binning, etc), which are essentially irrelevant for the present discussion.

The role of the centroid definition was discussed in [4], where the following remark was made (p. 6):

[...] it can be shown that *the mean is in principle completely achromatic*, i.e. in the limit of large s the curve would be completely flat. (The centre of gravity corresponds to the mean slope of the wavefront over the pupil. This is also the limiting value obtained with *any* symmetric estimator for $\lambda \rightarrow \infty$.) Thus, the chromaticity could in principle be eliminated by using the centre of gravity as the location estimator.

The main purpose of the present note is to provide the mathematical proof of the achromaticity of the centre of gravity (CoG), and to derive some useful results for practical centroid definitions, which of course in general *are* chromatic.

Similar notations as in previous notes will be used. In particular, (x, y) are linear coordinates in the pupil and (ξ, η) are angular coordinates in the image plane, with x and ξ in the along-scan direction. A rectangular pupil of dimension D along and H across scan is assumed. Monochromatic Fraunhofer diffraction at wavelength λ is considered, assuming the arbitrary wavefront error $W(x, y)$.

We are mainly interested in the monochromatic along-scan line-spread function (LSF) $L_\lambda(\xi)$, obtained by integrating the point-spread function (PSF) $P_\lambda(\xi, \eta)$ over η . The PSF and LSF are normalised to unit volume/area.

2 Definition of the centre of gravity (CoG)

The centre of gravity (CoG) of $L_\lambda(\xi)$ is naively defined as

$$\xi_0(\lambda) = \int_{-\infty}^{+\infty} L_\lambda(\xi) \xi \, d\xi, \quad (1)$$

remembering that $\int_{-\infty}^{+\infty} L_\lambda(\xi) \, d\xi = 1$ from the normalisation. For a sharp, rectangular pupil we have a problem, however, in that the integral in (1) is undefined. To see this, consider the LSF in the absence of WFE,

$$L_\lambda(\xi) = \frac{D}{\lambda} \operatorname{sinc}^2(\pi \xi D / \lambda), \quad (2)$$

where $\operatorname{sinc} x = \sin x / x$. For large x , the $\operatorname{sinc}^2 x$ function decreases as x^{-2} ; hence $\int_0^t x \operatorname{sinc}^2 x \, dx$ diverges as $t \rightarrow \infty$.² It can be noted that, *a fortiori*, higher moments of the diffraction image do not exist; e.g., the variance is infinite.

It is nevertheless possible to define the CoG (but not the higher moments) as the Cauchy Principal Value integral

$$\xi_0(\lambda) = \lim_{t \rightarrow \infty} \int_{-t}^{+t} L_\lambda(\xi) \xi \, d\xi, \quad (3)$$

²This argument applies to a sharp-edged rectangular pupil. An apodised pupil would produce more quickly declining wings, for which (1) converges.

since it will be found that the limiting value is independent of the choice of origin for ξ .

We now give an alternative, but presumably equivalent limiting definition of the CoG. Since $L_\lambda(\xi)$ is continuous and absolutely integrable, its Fourier transform

$$F_\lambda(f) = \int_{-\infty}^{+\infty} L_\lambda(\xi) \exp(-2\pi i f \xi) d\xi \quad (4)$$

exists for all spatial frequencies f (expressed in periods per radian). The imaginary part of F_λ is the sine transform

$$I_\lambda(f) = \int_{-\infty}^{+\infty} L_\lambda(\xi) \sin(-2\pi f \xi) d\xi, \quad (5)$$

which vanishes for $f = 0$. However, for sufficiently small but non-zero f the approximation $\sin(-2\pi f \xi) \simeq -2\pi f \xi$ will hold in a region of ξ where $L_\lambda(\xi)$ is significant. This suggests that the CoG could be defined as the limit of $I_\lambda(f)/(-2\pi f)$ as $f \rightarrow 0$. This is not shift invariant, but a slight modification takes care of that:

$$\xi_0(\lambda) = \lim_{f \rightarrow 0} \frac{\arg F_\lambda(f)}{-2\pi f}. \quad (6)$$

The 2π ambiguity of $\arg F_\lambda$ disappears when f is sufficiently small. Numerical calculations support the conjecture that (3) and (6) are equivalent.

3 The CoG in the presence of aberrations

We shall now derive an exact expression for CoG of the diffraction image in the presence of the arbitrary wavefront aberrations $W(x, y)$, based on the Fourier definition of the CoG in (6).

The Fourier transform of the line-spread function is in fact a well-known entity in optics, namely the optical transfer function (OTF) of the system – or rather a cut through the two-dimensional OTF at zero transverse spatial frequency. Some basic formulae are given in [3] and [5]. For convenience, the relevant equations are repeated here in current notation and properly normalised.

In the Fraunhofer approximation the monochromatic PSF is

$$P_\lambda(\xi, \eta) = \frac{1}{\lambda^2 DH} \left| \iint_{-\infty}^{+\infty} A(x, y) \exp[ik(x\xi + y\eta)] dx dy \right|^2, \quad (7)$$

where $k = 2\pi/\lambda$ is the wavenumber and A the complex pupil function,

$$A(x, y) = \begin{cases} \exp[ikW(x, y)] & \text{for } (x, y) \in \text{pupil} \\ 0 & \text{otherwise.} \end{cases} \quad (8)$$

Equation (7) is normalised such that $\iint P_\lambda(\xi, \eta) = 1$. An equivalent expression is

$$P_\lambda(\xi, \eta) = \frac{1}{\lambda^2} \iint_{-\infty}^{+\infty} O_\lambda(u, v) \exp[ik(u\xi + v\eta)] du dv, \quad (9)$$

where $O_\lambda(u, v)$ is the OTF, obtained as the normalised autocorrelation of the complex pupil function:

$$\begin{aligned} O_\lambda(u, v) &= \frac{1}{DH} \iint_{-\infty}^{+\infty} A\left(x + \frac{u}{2}, y + \frac{v}{2}\right) A^*\left(x - \frac{u}{2}, y - \frac{v}{2}\right) dx dy \\ &= \frac{1}{DH} \int_{-(H-|v|)/2}^{+(H-|v|)/2} \int_{-(D-|u|)/2}^{+(D-|u|)/2} \exp\left[ik\left\{W\left(x + \frac{u}{2}, y + \frac{v}{2}\right) - W\left(x - \frac{u}{2}, y - \frac{v}{2}\right)\right\}\right] dx dy. \end{aligned} \quad (10)$$

Note that $O_\lambda(0, 0) = 1$, and that $O_\lambda(u, v) = 0$ if $|u| \geq D$ or $|v| \geq H$. Conversely,

$$O_\lambda(u, v) = \iint_{-\infty}^{+\infty} P_\lambda(\xi, \eta) \exp[-ik(u\xi + v\eta)] d\xi d\eta. \quad (11)$$

The displacements u, v represent spatial frequencies expressed as linear measures through multiplication by the wavelength; in particular, $u = f\lambda$.

The corresponding formula for the monochromatic LSF,

$$L_\lambda(\xi) = \int_{-\infty}^{+\infty} P_\lambda(\xi, \eta) d\eta, \quad (12)$$

is readily obtained as

$$L_\lambda(\xi) = \frac{1}{\lambda} \int_{-\infty}^{+\infty} O_\lambda(u) \exp(iku\xi) du, \quad (13)$$

where

$$\begin{aligned} O_\lambda(u) &\equiv O_\lambda(u, 0) \\ &= \frac{1}{DH} \int_{-H/2}^{+H/2} \int_{-(D-|u|)/2}^{+(D-|u|)/2} \exp\left[ik\left\{W\left(x + \frac{u}{2}, y\right) - W\left(x - \frac{u}{2}, y\right)\right\}\right] dx dy. \end{aligned} \quad (14)$$

The inverse of (13) is

$$O_\lambda(u) = \int_{-\infty}^{+\infty} L_\lambda(\xi) \exp(-iku\xi) d\xi. \quad (15)$$

Comparing the last equation with (4) shows that $F_\lambda(f) = O_\lambda(u)$ if $2\pi f = ku$; hence (6) becomes

$$\xi_0(\lambda) = \lim_{u \rightarrow 0} \frac{\arg O_\lambda(u)}{-ku} \quad (16)$$

Now, expanding (14) in the limit of small u gives

$$\begin{aligned} O_\lambda(u) &= \frac{1}{DH} \int_{-H/2}^{+H/2} \int_{-D/2}^{+D/2} \exp\left[iku \frac{\partial W(x, y)}{\partial x}\right] dx dy \\ &= \frac{1}{DH} \int_{-H/2}^{+H/2} \int_{-D/2}^{+D/2} \left[1 + iku \frac{\partial W(x, y)}{\partial x}\right] dx dy \\ &= 1 + iku \frac{1}{DH} \int_{-H/2}^{+H/2} \left[W\left(+\frac{D}{2}, y\right) - W\left(-\frac{D}{2}, y\right)\right] dy, \end{aligned} \quad (17)$$

from which

$$\xi_0(\lambda) = -\frac{1}{DH} \int_{-H/2}^{+H/2} \left[W\left(+\frac{D}{2}, y\right) - W\left(-\frac{D}{2}, y\right) \right] dy \quad (18)$$

The right-hand side is simply the mean wavefront tilt along the pupil, which is clearly independent of λ . It follows that the along-scan CoG of the diffraction image is strictly achromatic. Exchanging the along and across-scan axes shows that the across-scan CoG is also achromatic, which is therefore true for the two-dimensional CoG as well.

4 Practical definitions of the centroid

4.1 Weight functions

The fact that the straightforward definition of the CoG in (1) does not work tells us something about the suitability of the CoG as a location estimator for diffraction images. It is in principle impossible to implement, since the LSF has infinite support, but even reasonably finite approximations are highly unsuitable, being unduly sensitive to noise in the most distant points which carry little signal.

Any practical implementation of the CoG calculation must consequently truncate the integral (or in practice, the sum) in (1) on both sides.³ To provide a centroid definition that is shift invariant, the truncation limits must follow the computed centroid; the equation to solve is therefore

$$\int_{\xi_0-t}^{\xi_0+t} L_\lambda(\xi)(\xi - \xi_0) d\xi = 0 \quad (19)$$

assuming symmetric clipping at distance t from the centroid.

The truncation limit t can be chosen to minimise the variance of the resulting location estimate in the presence of noise. For the non-aberrated case of (2), in the bright-star limit and considering photon noise only, it is found that the optimal truncation is obtained for $t = \lambda/D$, corresponding to the first diffraction minimum (cf. [1]). The resulting estimator turns out to be rather good estimator in the bright-star limit, but less suitable for fainter images where background and read-out noise become significant. The sharp truncation is however difficult to implement accurately for sampled data.

Equation (19) can be cast in the more general form an M-estimate of the location ([8], Ch. 15.7),

$$\int_{-\infty}^{+\infty} L_\lambda(\xi)\psi(\xi - \xi_0) d\xi = 0, \quad (20)$$

where

$$\psi(z) = \begin{cases} z & \text{if } |z| < t \\ 0 & \text{otherwise} \end{cases} \quad (21)$$

is the so-called weight function associated with the M-estimate. Most of the practical centroid definitions can be cast in this form, but using different weight functions [1]. For

³We should avoid using the term ‘centre of gravity’ for such modified definitions of the location. Henceforth, the term ‘centroid’ will be used for the more general concept, while CoG is reserved for the particular centroid discussed in Sects. 2 and 3.

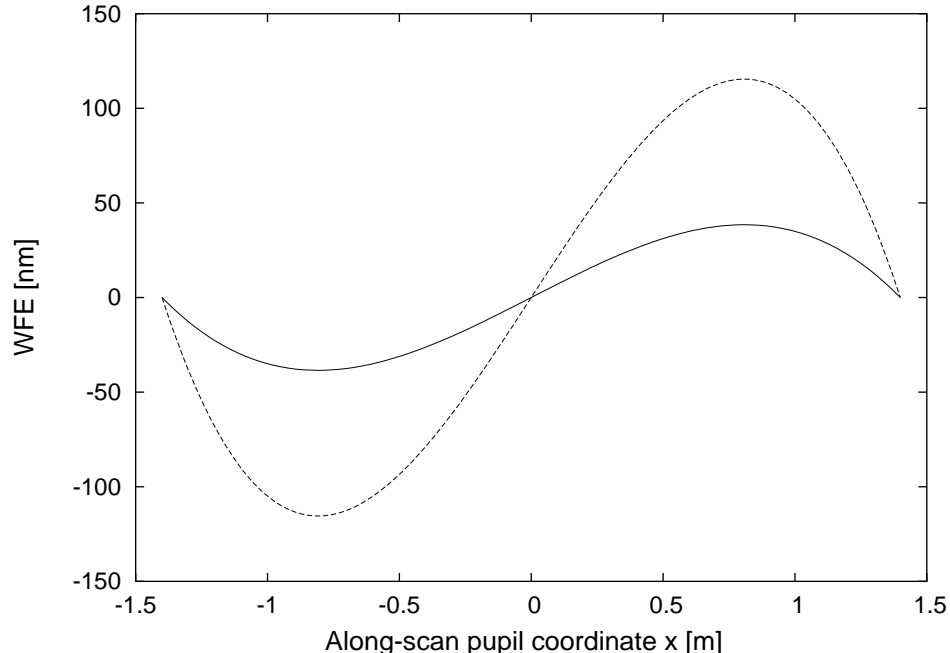


FIGURE 1: Assumed WFE for the two test cases with results in Fig. 2. The solid curve is for (24) with $c = 100$ nm, the dashed curve is for $c = 300$ nm. The mean tilt is, respectively, 11.79 mas and 35.36 mas. The RMS wavefront error after removing the tilt is 15.2 nm and 45.4 nm. Other optical parameters are: $D = 1.4$ m, focal length = 46.7 m, along-scan pixel size = $10 \mu\text{m}$.

example, least-squares fitting a gaussian of standard width s is equivalent to solving (20) with

$$\psi(z) = z \exp(-z^2/2s^2). \quad (22)$$

Similarly, the maximum-likelihood location estimate in the presence of noise with variance proportional to $g(\xi) = b + aL(\xi)$ corresponds to the weight function

$$\psi(z) = \frac{g'(z)}{g(z)} \quad (23)$$

(see [1]), and so on. Optimum weight functions tend to have a linear region around $z = 0$ and a smooth transition to zero some distance beyond the points of the maximum slope of $L(\xi)$.

4.2 Chromatic behaviour of practical centroids

Experience with several practical centroid definitions shows that they always exhibit some degree of chromatic behaviour, which however tends to decrease when the linear region of the weight function is extended, e.g. by using a larger standard width for the fitted gaussian. In light of the theoretical results of Sect. 3 we conclude that the chromatic behaviour is caused by the deviation of any practical weight function from the theoretical

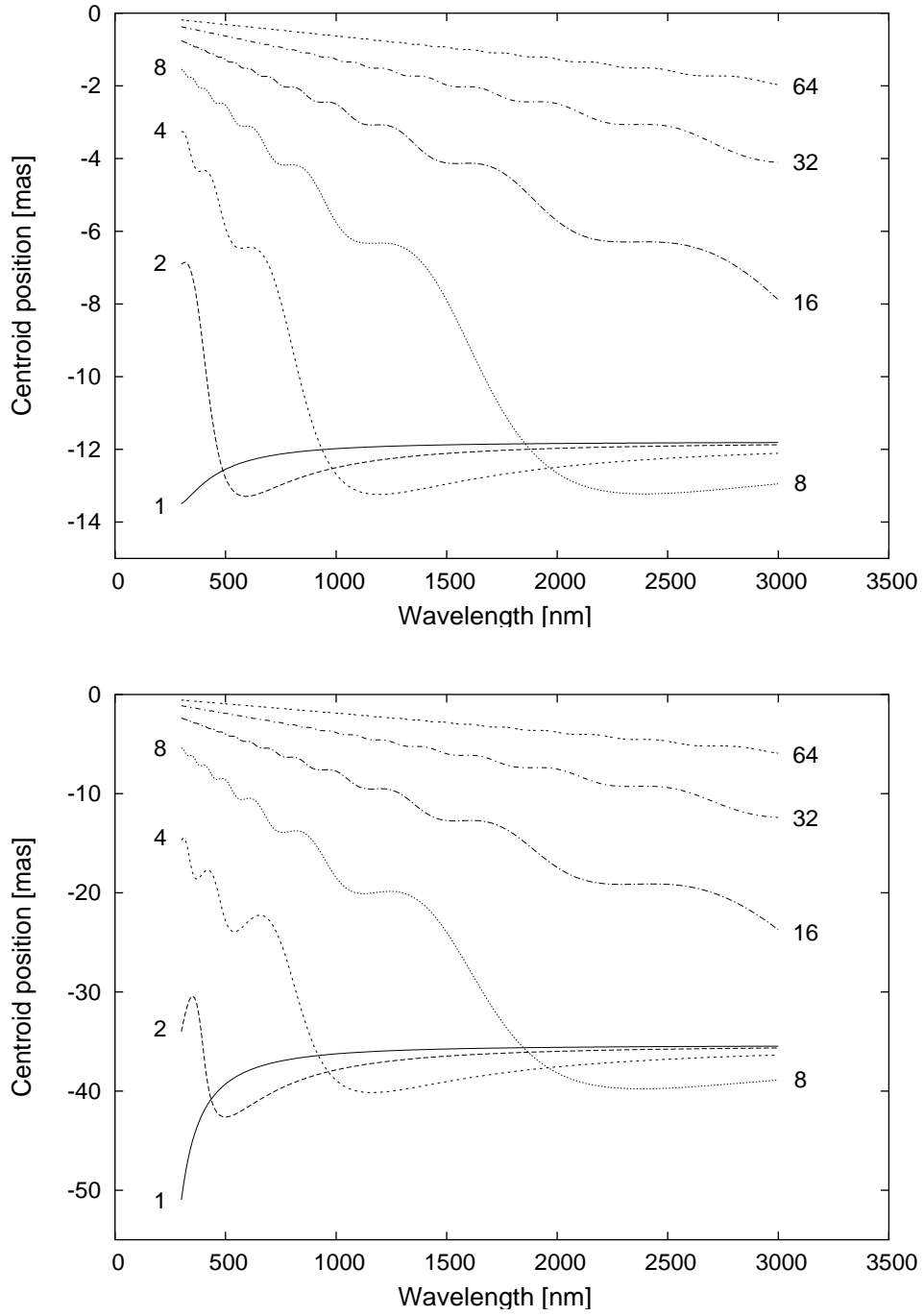


FIGURE 2: Examples of the behaviour of the monochromatic centroid defined by the truncated mean (21) for the WFE cases shown in Fig. 1. The upper panel is for the WFE shown as a solid curve in Fig. 1; the lower panel corresponds to the dashed curve in Fig. 1. The curves are labelled by the truncation width t expressed in pixels (1 pixel = 44.2 mas). A realistic centroid definition for Gaia will have $t \simeq 2$ pixels.

CoG weight function, $\psi(z) \propto z$, and in particular by the need to truncate the weight function or smoothly reduce it to zero for $|z| \gtrsim \lambda/D$.

Another empirical result is that the curves of centroid position versus wavelength tend to flatten out towards longer wavelength (e.g., Figs. 1–2 in [4] and Fig. 1 in [6]). This behaviour may be qualitatively understood as follows. Increasing the wavelength eventually makes the wavefront errors negligible in the sense that the image approaches the non-aberrated diffraction image. To light of such long wavelengths, the wavefront appears to be ‘flat’, and could just as well be represented by the tilted plane wavefront that best agrees with the actual wavefront. In the limit of infinite wavelength, the centroid position therefore corresponds to the tilt of a plane fitted (in the least-squares sense) to the actual wavefront.

In order to illustrate the behaviour of a centroid defined by a weight function of finite range, Figs. 1–2 show some representative results using the truncated mean in (21). Figure 1 shows the assumed wavefront errors, which are purely cubic functions in the along-scan pupil coordinate x ,

$$W(x, y) = c \left(\frac{2x}{D} \right) \left[1 - \left(\frac{2x}{D} \right)^2 \right], \quad (24)$$

with $c = 100$ nm and 300 nm. It can be noted that $W(-D/2, y) = W(+D/2, y)$ in both cases, which means that the theoretical CoG is at the origin ($\xi = 0$). Figure 2 shows the resulting centroids as function of wavelength and truncation limit t (expressed in pixels).

Figure 2 confirms the theoretical result of Sect. 3 that the CoG is approached for $tD/\lambda \rightarrow \infty$, which happens either when $\lambda \rightarrow 0$ or $t \rightarrow \infty$.

It also shows (at least for the smaller values of t) that, for fixed and finite t , the centroid approaches the value corresponding to the mean wavefront tilt (approximately -12 mas and -36 mas, respectively) in the long-wavelength limit.

The behaviour between these two extremes is somewhat complex, but the main trend is that the centroid deviates from the CoG by an amount roughly proportional to λ and inversely proportional to t . The transition from this quasi-linear dependence on wavelength and the approximately flat curves at the mean wavefront tilt occurs at $\lambda \simeq tD$. As previously pointed out, in the presence of photon noise it is desirable to choose $t \simeq \lambda/D$ (or slightly less if background and readout noise is significant); therefore it seems inevitable that real centroid definitions will operate in the vicinity of the transition region, where the chromatic behaviour is nonlinear in wavelength. For example, with current Gaia parameters and an effective wavelength around 600 nm, the optimum truncation is $t \simeq 88$ mas $\simeq 2$ pixels. And the curve for $t = 2$ in Fig. 2 is not nice!

A final remark: The statement in [4], quoted in Sect. 1 above, was incorrect in assuming that the CoG is obtained in the long-wavelength limit. The phrase ‘mean slope of the wavefront over the pupil’ is in fact ambiguous, and could be understood both as the expression on the right-hand side of (18) and as the best-fitting plane. It is probable that the error in [4] was caused by a confusion of the two concepts.

5 Conclusions

The main conclusions of this investigation are:

1. For a sharp rectangular pupil, the centre-of-gravity (CoG) of the diffraction image can only be defined as a limiting value obtained by including the far wings. Thus, in the real world, and in particular in the presence of background noise, it cannot be practically realised. Figure 2 shows that, for Gaia, the averaging would have to cover a far larger area than the actually sampled windows in order to approximate the CoG.
2. Nevertheless, the theoretical CoG has the interesting property that it is strictly achromatic for arbitrary wavefront errors. The position of the CoG corresponds to the mean wavefront slope along the pupil as defined by (18).
3. Practically useful centroiding algorithms can be described by weight functions $\psi(z)$ that have a finite range (say, of order $\pm t$) around the centroid. They exhibit chromatic behaviour which depends in a complex way on the particular weight function and wavefront errors. In the limit of large t or small λ , the CoG is obtained. In the long-wavelength limit the centroid position is instead given by the best-fitting tilted plane wavefront. The transition between the two behaviours occurs at $\lambda \simeq tD$. Centroid definitions that are optimal with respect to noise tend to operate precisely in this (strongly non-linear) transition region.

References

- [1] Lindegren L., 1978: *Photoelectric astrometry: A comparison of methods for precise image location*, in F.V. Prochazka & R.H. Tucker (eds.), *Modern Astrometry*, IAU Coll. No. 48, University Observatory Vienna, p. 197
- [2] Lindegren L., 1998: *Chromatic displacement versus spectral energy distribution*, SAG-LL-016 (27 March 1998)
- [3] Lindegren L., 1998: *Calculation of chromatic displacement*, SAG-LL-024 (25 October 1998)
- [4] Lindegren L., 2001: *GAIA chromaticity calibration and design of the Broad Band Photometry system*, GAIA-LL-039 (13 June 2001)
- [5] Lindegren L., 2001: *Representation of LSF and PSF for GDAAS-2*, GAIA-LL-046 (2 May 2003)
- [6] Lindegren L., 2003: *Gaia chromaticity calibration and the BBP filter shape*, GAIA-LL-049 (15 November 2003)
- [7] Lindegren L., 2004: *Chromaticity specification*, GAIA-LL-053, Ver. 1 (8 May 2004)
- [8] Press W.H., Flannery B.P., Teukolsky S.A., Vetterling W.T., 1992: *Numerical recipes in Fortran*, Cambridge University Press (free on-line version available at <http://www.nr.com/>)